JACS
JOURNAL OF THE AMERICAN CHEMICAL SOCIETY
pubs.acs.org/JACS
Article

Chiral Macrocycles for Enantioselective Recognition

Guang Sun, Xue Zhang, Zhe Zheng, Zhi-Yuan Zhang,* Ming Dong,* Jonathan L. Sessler,* and Chunju Li*

Cite This: J. Am. Chem. Soc. 2024, 146, 26233−26242
Read Online
ACCESS | Metrics & More | Article Recommendations | Supporting Information

ABSTRACT: The efficient synthesis of chiral macrocycles with highly enantioselective recognition remains a challenge. We have addressed this issue by synthesizing a pair of chiral macrocycles, namely, *R*/*S*-BINOL[2], achieving total isolated yields of up to 62% through a two-step reaction sequence. These macrocycles are readily purified by column chromatography over silica gel without the need for chiral separation, thus streamlining the overall synthesis. *R*/*S*-BINOL[2] demonstrated enantioselective recognition toward chiral ammonium salts, with enantioselectivity (K_S/K_R) values reaching up to 13.2, although less favorable separations were seen for other substrates. *R*/*S*-BINOL[2] also displays blue circularly polarized luminescence with a $|g_{lum}|$ value of up to 2.2×10^{-3}. The *R*/*S*-BINOL[2] macrocycles of this study are attractive as chiral hosts in that they both display enantioselective guest recognition and benefit from a concise, high-yielding synthesis. As such, they may have a role to play in chiral separations.

INTRODUCTION

Chiral recognition continues to receive attention due to its crucial role in understanding biological processes,[1−4] aiding pharmaceutical design,[5,6] creating asymmetrically catalytic systems,[7−12] and preparing chiral separation materials.[13−17] Efforts have long been devoted to the design and development of chiral recognition tools, including chiral small organic molecules,[18−24] helical supramolecular assemblies,[25−29] chiral porous materials,[30−33] and chiral polymers.[34−37] Within this set, macrocyclic compounds, such as crown ethers,[38−41] cyclodextrins,[42−44] calixarenes,[45−48] cucurbiturils,[49−52] and other macrocyclic hosts,[53−60] are viewed as being particularly attractive for chiral recognition due to their preorganized cavities and the presence of multiple binding sites (Table S1). Some chiral macrocycles, such as chiral crown ethers and cyclodextrins, have even been commercialized for chiral separations.[61−64] However, there are still key issues that need to be addressed. First, the enantioselectivity ($K_{R(S)}/K_{S(R)}$ or $K_{L(D)}/K_{D(L)}$), a critical parameter reflecting the chiral recognition capability, is lower than 5 for most reported chiral macrocycles.[59,65−68] Enantioselectivities greater than 10 are thus rare, although progress beyond this limit has been reported in recent years. For instance, Chen et al. reported an enantioselective recognition of 12.9 in water using chiral macrocyclic octopus[3]arenes.[69] Lledó and coworkers reported a chiral cavitand receptor with a K_S/K_R value of 18.7.[47] Yang and Jiang synthesized a chiral naphthotubes that display an enantioselectivity value of 34.4.[70] Cai and coworkers developed a water-soluble conjugated macrocycle that provided enantioselectivities up to 18.7.[71] Second, the preparation of chiral macrocycles is generally limited by tedious syntheses, low yields (generally under 20% overall), and a need to preseparate the chiral forms before use. Collectively, these limitations can be an impediment to practical applications. There thus remains a need for chiral macrocyclic receptors that simultaneously possess high enantioselectivity (K_S/K_R > 10) and benefit from concise, high-yielding syntheses (Table S1 and Figure S1). Here, we report a set of binaphthol macrocycles that are readily prepared in two synthetic steps in yields exceeding 60% and which act as effective chiral hosts for chiral ammonium salts.

The present study is based on our recent development of a modular method for the preparation of functional macrocycles and endobinding site macrocycles.[72,73] Binaphthols were chosen as the chiral units due to their long-standing use as chiral recognition elements in host−guest chemistry.[23,38,74] By incorporating binaphthol subunits into our syntheses, we

Received: June 11, 2024
Revised: September 4, 2024
Accepted: September 5, 2024
Published: September 13, 2024

https://doi.org/10.1021/jacs.4c07924
J. Am. Chem. Soc. 2024, 146, 26233−26242

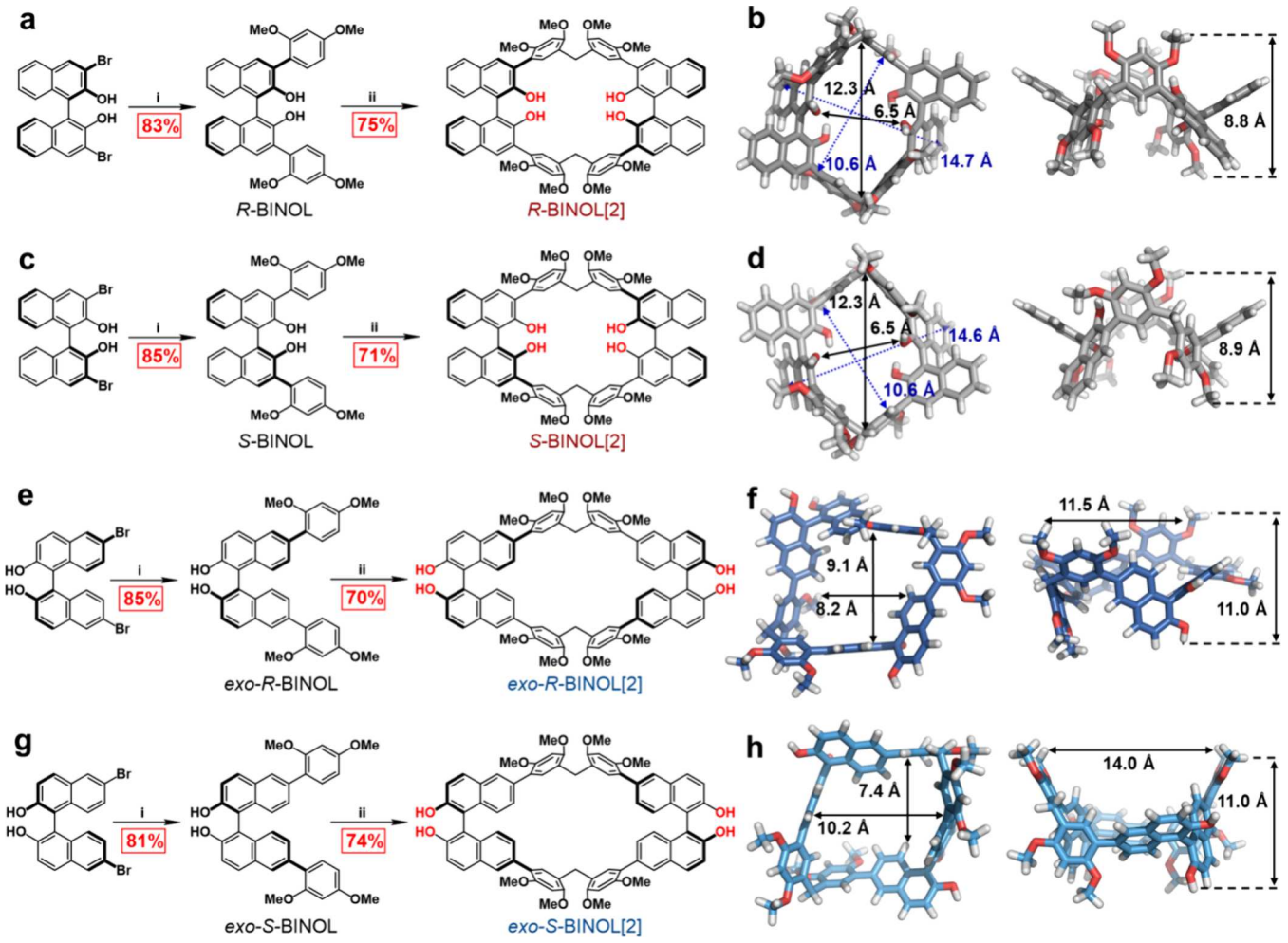

Figure 1. (a, c, e, g) Synthesis of (a) *R*-BINOL[2], (c) *S*-BINOL[2], (e) *exo*-*R*-BINOL[2], and (g) *exo*-*S*-BINOL[2] reaction conditions: (i) 2,4-dimethoxybenzeneboronic acid, $Pd(PPh_3)_4$ or $Pd(dppf)Cl_2$, Na_2CO_3, 1,4-dioxane/H_2O, under N_2, reflux, 12−18 h and (ii) $(CH_2O)_n$, $BF_3{\cdot}Et_2O$, CH_2Cl_2, r.t., 5 min). (b, d) Single-crystal structures of (b) *R*-BINOL[2] and (d) *S*-BINOL[2] (CCDC numbers 2338090 and 2338097). (f, h) Calculated structures of (f) *exo*-*R*-BINOL[2] and (h) *exo*-*S*-BINOL[2] shown in the top and side views. Color codes: C, gray or blue; O, red; H, white.

postulated that it would be possible to create a new class of easy-to-prepare chiral hosts. In particular, the presence of four OH groups directed inward was expected to provide directional binding sites that would favor stereochemically selective guest binding. Furthermore, the direct connection between the recognition sites (OH) and the chiral moieties (binaphthyls) might enhance chiral transfer between the hosts and guests, thereby increasing the enantioselectivity. Finally, by utilizing 2,4-dimethoxyphenyl, which has demonstrated high activity and possesses fixed reaction sites, as a reaction component, we anticipated that a high-yielding synthesis could be achieved. The present study was undertaken as a test of this hypothesis.

As shown in Figure 1, two pairs of binaphthol macrocycles, namely, *R*/*S*-BINOL[2] and *exo*-*R*/*S*-BINOL[2], were synthesized in yields up to 62% in two steps from commercially available starting materials. Purification of the homochiral macrocycles was achieved by column chromatography using a simple silica gel column without the need for chiral separation. The macrocycles possessing inward-directing OH groups, (*R*/*S*-BINOL[2]), demonstrated high enantioselective recognition toward chiral ammonium salts, with a K_R/K_S up to 13.2 (vide infra). It was discovered that the structures of the guests dictate the enantioselectivity with K_R/K_S values of only about 2 being seen for unsuitable guests. The *exo*-*R*/*S*-BINOL[2] congeners were also studied. They were found to lack any appreciable recognition capacity, presumably because of the absence of inward-pointing OH groups. To our knowledge, chiral macrocycles *R*/*S*-BINOL[2] are the first of their kind to benefit simultaneously from three useful features, namely, a concise synthesis process giving overall yields exceeding 60%, an ability to be used directly without preseparation of enantiomers, and effective substrate recognition characterized by high enantioselectivity ($K_S/K_R > 10$). We thus believe that the present set of chiral macrocycles may see use in chiral separations.

RESULTS AND DISCUSSION

Synthesis and Characterization of Chiral Macrocyclic Hosts *R*/*S*-BINOL[2] and *Exo*-*R*/*S*-BINOL[2]. The *R*-BINOL monomer was synthesized in 83% yield through a Suzuki−Miyaura cross-coupling reaction between commercially available *R*-3,3′-dibromo-1,1′-bi-2-naphthol and 2,4-dimethoxyphenylboronic acid (Figures 1a, S2−S4, and Scheme S1). The cyclization of the monomer to form the macrocyclic host *R*-BINOL[2] was achieved in 75% yield by condensing it with

https://doi.org/10.1021/jacs.4c07924
J. Am. Chem. Soc. 2024, 146, 26233−26242

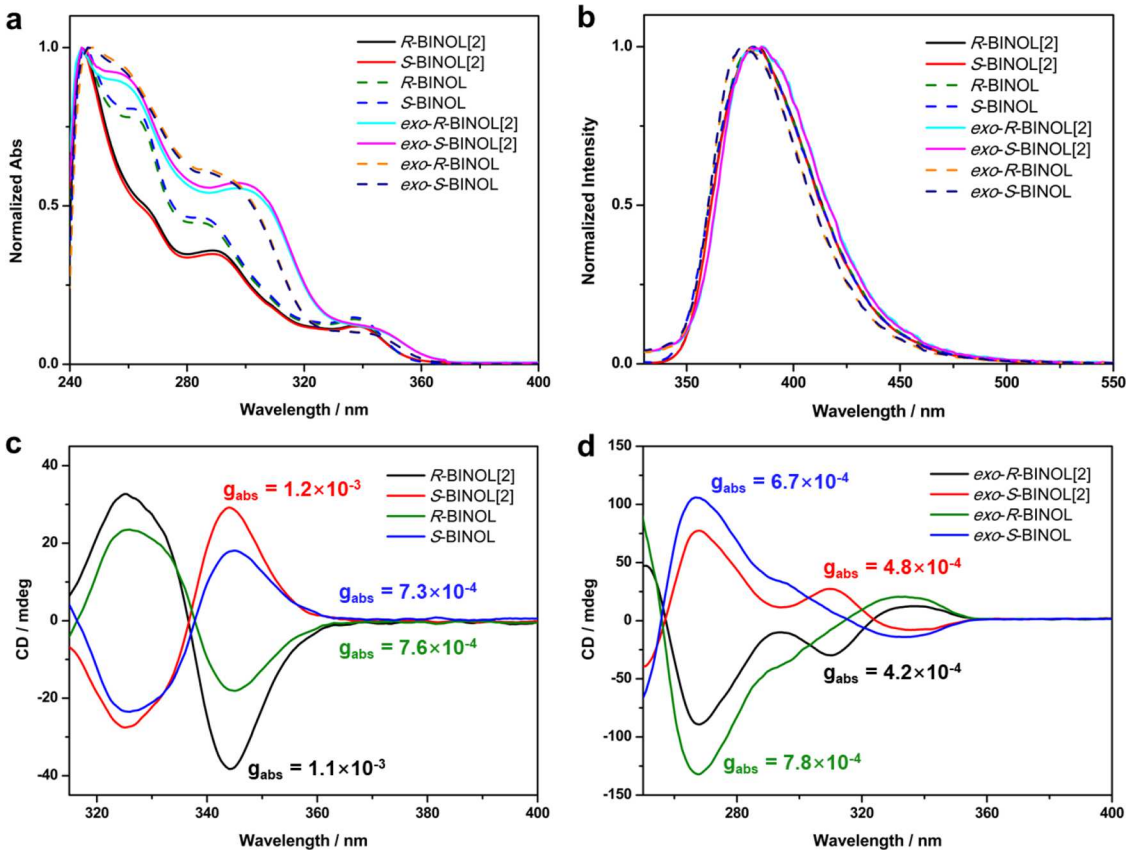

Figure 2. (a) Normalized UV/vis absorption spectra and (b) photoluminescence emission spectra of *R*/*S*-BINOL[2], *R*/*S*-BINOL, *exo*-*R*/*S*-BINOL[2], and *exo*-*R*/*S*-BINOL. (c, d) CD spectra of (c) *R*/*S*-BINOL[2] and *R*/*S*-BINOL and (d) *exo*-*R*/*S*-BINOL[2] and *exo*-*R*/*S*-BINOL ([*R*/*S*-BINOL] = [*exo*-*R*/*S*-BINOL] = 2[*R*/*S*-BINOL[2]] = 2[*exo*-*R*/*S*-BINOL[2]] = 2×10^{-5} mol/L for UV/vis spectra, 1×10^{-5} mol/L for photoluminescence spectra, 1×10^{-4} mol/L for CD spectra in $CHCl_3$, E_x = 300 nm.

paraformaldehyde in dichloromethane (DCM) at room temperature in the presence of a catalytic amount of $BF_3 \cdot Et_2O$ (Figures 1a, S5−S9, and Scheme S2). This cyclization can also be carried out in other solvents, such as 1,2-dichloroethane (DCE) and $CHCl_3$, and using other catalysts, including trifluoromethanesulfonic acid (TfOH), *p*-toluenesulfonic acid (TsOH), trifluoroacetic acid (TFA), and $FeCl_3$ (Table S2). The enantiomer *S*-BINOL[2] was prepared from *S*-BINOL in 71% yield by using the same basic procedure as was used for *R*-BINOL[2] (Figure 1c). Macrocycles with outward-directed OH groups were synthesized in 70% (*exo*-*R*-BINOL[2]) and 74% (*exo*-*S*-BINOL[2]) cyclization yields, respectively, using a method similar to that used for *R*/*S*-BINOL[2] (Figures 1e,g, S10−S15, Schemes S3, and S4).

Diffraction grade colorless single crystals of *R*/*S*-BINOL[2] were obtained through the slow evaporation of an acetonitrile solution containing the macrocyclic hosts at room temperature for 4 days. The resulting single-crystal structures are shown in Figure 1 with associated data given in Table S3. Macrocycle *R*-BINOL[2] adopts a funnel-shaped conformation in the solid state, characterized by a rhombic inner cavity with dimensions of 12.3 Å × 6.5 Å, an outer cavity size measuring 14.7 Å × 10.6 Å, and a cavity depth of 8.8 Å (Figure 1b). Four vertically aligned 2,4-dimethoxyphenyl groups alternating in opposite directions help define a deep 3D cavity that appears well-suited for substrate binding. Individual molecules of *R*-BINOL[2] stack in register with other molecules via presumed C−H···π and C−H···O interactions, yielding infinite empty channels within the crystal (Figure S16a−c). Enantiomer *S*-BINOL[2] displays analogous conformational attributes, cavity size, and superstructural features (Figures 1d and S16d−f). Although single crystals of *exo*-*R*/*S*-BINOL[2] could not be obtained, their energy-minimized structures were inferred based on DFT (B3LYP/6-31G(d)) calculations. Notably, both *exo*-*R*-BINOL-[2] and *exo*-*S*-BINOL[2] contain box-like cavities, characterized by dimensions of 9.1 Å × 8.2 Å and 10.2 Å × 7.4 Å, respectively, as well as larger outer cavities with dimensions of 11.5 Å by 14.0 Å while displaying a uniform depth of 11.0 Å (Figure 1f,h).

Surface electrostatic potential maps were constructed. They revealed that all four macrocyclic hosts possess electron-rich cavities, lending support to the suggestion that they would act as effective receptors for electron-deficient guest molecules (Figure S17).

The photophysical properties of *R*/*S*-BINOL[2], *R*/*S*-BINOL, *exo*-*R*/*S*-BINOL[2], and *exo*-*R*/*S*-BINOL were also investigated. These molecules exhibited similar absorption features, with prominent bands being seen between 260 and 370 nm in $CHCl_3$; presumably, this reflects the presence of similar chromophores (Figure 2a). In particular, the emission spectrum of *R*-BINOL[2] was characterized by a fluorescent emission peak at 387 nm in $CHCl_3$ characterized by a photoluminescent quantum yield (PLQY) of 8.4%. The increase in PLQY relative to *R*-BINOL, for which a value of 4.5% was recorded, is ascribed to a macrocyclization-induced emission enhancement effect (Figures 2b and S18).[75] *Exo*-*R*-

https://doi.org/10.1021/jacs.4c07924
J. Am. Chem. Soc. 2024, 146, 26233−26242

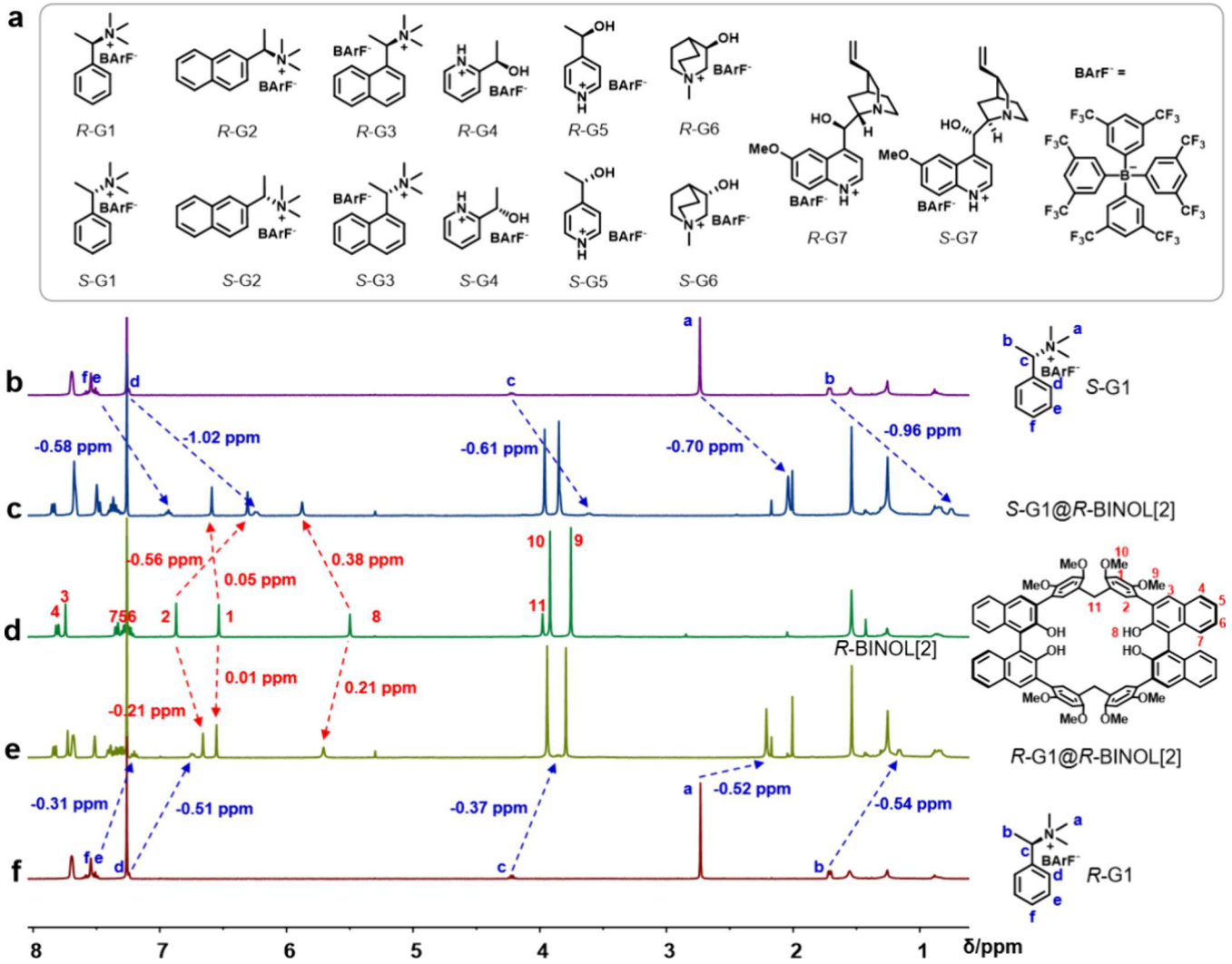

Figure 3. (a) Chemical structures of the guests. (b–f) ^{1}H NMR spectra (400 MHz, $CDCl_3$, 2.00 mM, 298 K) of (b) *S*-G1, (c) *S*-G1@*R*-BINOL[2], (d) *R*-BINOL[2], (e) *R*-G1@*R*-BINOL[2], and (f) *R*-G1. Changes in the chemical shifts are marked in red for the host and blue for the guests

BINOL[2] exhibited similar fluorescence and emission features (PLQY = 7.9%) (Figures 2b and S19).

The chiroptical properties of this set of the present BINOL-containing macrocycles were further investigated by using circular dichroism (CD) spectroscopy. As shown in Figure 2c, *R*-BINOL[2] showed positive-to-negative Cotton bands in the 315 to 365 nm spectral range in $CHCl_3$, while *S*-BINOL[2] exhibited a mirror-image CD spectrum. The absorption dissymmetry factors ($|g_{abs}|$) of *R*-BINOL[2] at 344 nm is 1.1×10^{-3}, a value significantly greater than displayed by its constituent, monomer *R*-BINOL ($|g_{abs}| = 7.6 \times 10^{-4}$) (Figure 2c). Similar increases were seen for macrocycle *S*-BINOL[2] ($|g_{abs}| = 1.2 \times 10^{-3}$) and monomer *S*-BINOL ($|g_{abs}| = 7.3 \times 10^{-4}$). Macrocycles *exo*-*R*/*S*-BINOL[2] and their corresponding constituents, *exo*-*R*/*S*-BINOL, also displayed distinct CD spectra (Figure 2d). Both enantiomers exhibited mirror image CD spectra in the 255–355 nm spectral range in $CHCl_3$, with relatively weak $|g_{abs}|$ values of 4.2×10^{-4} and 4.8×10^{-4} being recorded for *exo*-*R*-BINOL[2] and *exo*-*S*-BINOL[2], respectively. These latter values are on the same order of magnitude as those of their corresponding monomers ($|g_{abs}| = 7.8 \times 10^{-4}$ for *exo*-*R*-BINOL and 6.7×10^{-4} for *exo*-*S*-BINOL). Taken in concert, these results provide additional evidence for the enantiotropy of the macrocyclic structures and their enantiopurity. Moreover, both pairs of enantiomeric macrocycles exhibited mirror image circularly polarized luminescence (CPL) in the 350 to 450 nm range in $CHCl_3$, with luminescence dissymmetry factors ($|g_{lum}|$) on the order of 2.2×10^{-3} (Figure S20).

Enantioselective Recognition. Due to their electron-rich cavities, the chiral macrocycles of this study were considered likely to act as hosts for electron-withdrawing guests. To investigate their enantioselective binding capabilities, we studied their interactions with six pairs of chiral cationic guests. As an example, *R*/*S*-G1 was separately mixed with equimolar quantities of *R*-BINOL[2] in $CDCl_3$. This mixing produced readily discernible changes in the proton signals of both the hosts and guests (Figure 3b–f). All of the proton signals of *R*/*S*-G1 shifted upfield, a finding taken as evidence of a strong shielding effect induced as the result of complexation by host *R*-BINOL[2]. Furthermore, with *R*-BINOL[2], larger changes were seen in the proton signals of *S*-G1 than in the case of *R*-G1 ($\Delta\delta$ = −0.70 and −0.52 ppm for H_a, −0.96 and −0.54 ppm for H_b, −0.61 and −0.37 ppm for H_c, −1.02 and

https://doi.org/10.1021/jacs.4c07924
J. Am. Chem. Soc. 2024, 146, 26233–26242

Table 1. Association Constants (K_a/M^{-1}) of *R*/*S*-BINOL[2] for Chiral Cationic Guests *R*/*S*-G1−G7, as Determined by ^{1}H NMR Spectroscopic Titrations in $CDCl_3$ or CD_2Cl_2 at 298 K for *R*/*S*-G1−G3 and *R*/*S*-G6−G7, and by Fluorescence Titrations in $CHCl_3$ at 298 K for *R*/*S*-G4−G5[a]

		R-BINOL[2]		*S*-BINOL[2]	
entry	guests	K_a/M^{-1}	K_R/K_S	K_a/M^{-1}	K_R/K_S
1	*R*-G1	$(1.3 \pm 0.1) \times 10^3$	1/11.5	$(1.4 \pm 0.3) \times 10^4$	10.8/1
2	*S*-G1	$(1.5 \pm 0.3) \times 10^4$		$(1.3 \pm 0.2) \times 10^3$	
3	*R*-G2	$(3.8 \pm 0.4) \times 10^3$	1/13.2	$(4.1 \pm 0.3) \times 10^4$	13.2/1
4	*S*-G2	$(5.0 \pm 0.6) \times 10^4$		$(3.1 \pm 0.3) \times 10^3$	
5	*R*-G3	$(3.2 \pm 0.7) \times 10^3$	2.5/1	$(1.0 \pm 0.1) \times 10^3$	1/1.7
6	*S*-G3	$(1.3 \pm 0.2) \times 10^3$		$(1.7 \pm 0.4) \times 10^3$	
7[b]	*R*-G4	$(1.3 \pm 0.1) \times 10^6$	4.4/1	$(2.2 \pm 0.2) \times 10^5$	1/3.8
8[b]	*S*-G4	$(3.0 \pm 0.3) \times 10^5$		$(8.3 \pm 1.1) \times 10^5$	
9[b]	*R*-G5	$(3.6 \pm 0.3) \times 10^5$	1/2.0	$(5.9 \pm 0.4) \times 10^5$	2.2/1
10[b]	*S*-G5	$(7.4 \pm 0.7) \times 10^5$		$(2.8 \pm 0.3) \times 10^5$	
11	*R*-G6	$(7.1 \pm 1.1) \times 10^3$	2.2/1	$(3.2 \pm 0.6) \times 10^3$	1/2.2
12	*S*-G6	$(3.3 \pm 0.5) \times 10^3$		$(6.9 \pm 0.6) \times 10^3$	
13[c]	*R*-G7	$(5.0 \pm 0.4) \times 10^2$	1/2.4	$(1.3 \pm 0.2) \times 10^3$	2.5/1
14[c]	*S*-G7	$(1.2 \pm 0.3) \times 10^3$		$(5.2 \pm 0.6) \times 10^2$	

[a]Error values represent the standard deviations determined from three independent measurements. [b]In these cases, the K_a values were determined by fluorescence spectral titrations because they exceed 10^5 M^{-1} and could not be accurately calculated from data acquired by means of ^{1}H NMR spectroscopic titrations. [c]^{1}H NMR spectral titrations were conducted in CD_2Cl_2 due to the poor solubility of G7 in $CDCl_3$.

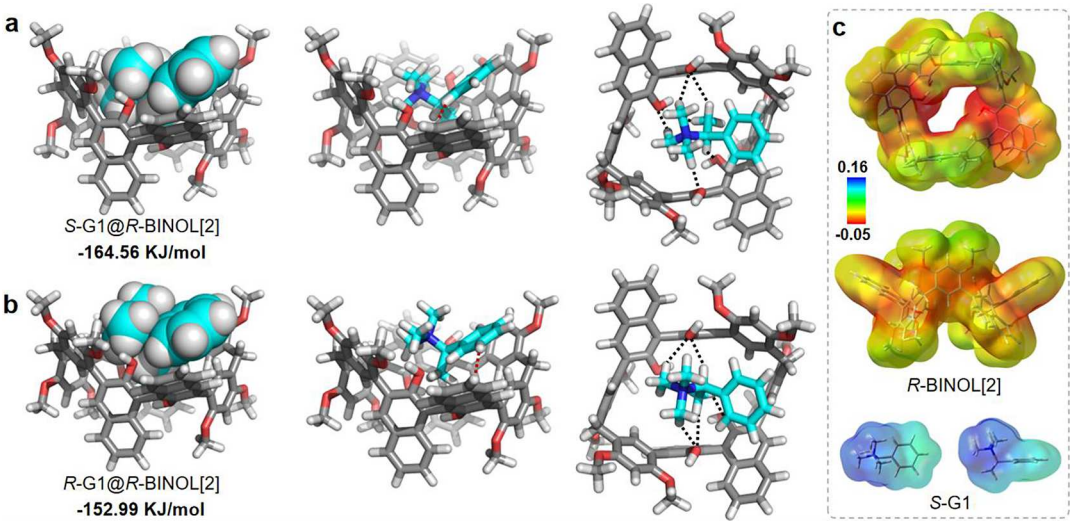

Figure 4. (a, b) Optimized binding geometry of (a) *S*-G1@*R*-BINOL[2] and (b) *R*-G1@*R*-BINOL[2] host−guest complexes in side and top views obtained by DFT calculations. (c) MEP-mapped molecular van der Waals surfaces of *R*-BINOL[2] and *S*-G1 in top and side views. Note: the red region represents a negative potential area characterized by an abundance of electrons. Blue region represents a positive potential area characterized by a relative absence of electrons.

−0.51 ppm for H_d, and −0.58 and −0.31 ppm for H_e). This is expected for a recognition process that benefits from the chiral discrimination induced by *R*-BINOL[2]. Downfield shifts in the OH proton signals of *R*-BINOL[2] were also seen, leading us to suggest that these groups are involved in the hydrogen bonding-based recognition of the presumably bound guests. Again, a guest dependence was seen with $\Delta\delta$ values for these signals of 0.38 for *S*-G1 and 0.21 ppm for *R*-G1 being observed. As above, this was taken as evidence of enantioselective binding. Gratifyingly, corresponding, if mirror image-like, effects were seen in the case of enantiomer *S*-BINOL[2] and guests *S*-G1 and *R*-G1 (Figure S21). In the ROESY spectra of *R*-G1@*R*-BINOL[2], cross-peaks between H_a−H_2 and H_a−H_8 were readily apparent. In the case of complex *S*-G1@*R*-BINOL[2], in addition to these NOE peaks, cross-peaks between H_e−H_{10} were also observed (Figures S22−S25). These findings are taken as evidence for the close proximity between the trimethylammonium group of the guest and the OH/2,4-dimethoxyphenyl moiety of the host. This, in turn, leads us to suggest the presence of hydrogen bonding interactions between *S*/*R*-G1 and *R*-BINOL[2].

Job's plots were constructed by changing the ratio of the host to the guest and measuring the chemical shifts of key proton signals of the host. These plots revealed maximal changes in the chemical shifts at a mole fraction of 0.5. While not a proof, such findings are consistent with a binding stoichiometry of 1:1 between *R*/*S*-G1 and *R*/*S*-BINOL[2] (Figure S26). This inferred stoichiometry was further supported by the observation of a prominent peak corresponding to [*S*/*R*-G1@*R*/*S*-BINOL[2]-BArF]$^+$ in the high-resolution mass spectra of the putative host−guest complexes (Figure S27).

https://doi.org/10.1021/jacs.4c07924
J. Am. Chem. Soc. 2024, 146, 26233−26242

Assuming a 1:1 binding stoichiometry, the association constants and enantioselectivities were determined based on ^{1}H NMR spectroscopic titrations. Typically, enantioselectivities can be assessed by allowing either one chiral host to interact with both enantiomers of a nonracemic guest or testing how the two enantiomers of a chiral host interact with a single enantiomer of the guest. The enantioselectivities derived from both approaches should prove consistent. Given that complexes *R*-G1@*R*-BINOL[2] and *R*-G1@*S*-BINOL[2] are enantiomers of complexes *S*-G1@*S*-BINOL[2] and *S*-G1@*R*-BINOL[2], respectively, we expected that the association constants would prove similar.

In the present instance, ^{1}H NMR spectroscopic titrations (conducted in triplicate) yielded association constants of $(1.3 \pm 0.1) \times 10^3$ M^{-1} for *R*-G1@*R*-BINOL[2] and $(1.5 \pm 0.3) \times 10^4$ M^{-1} for *S*-G1@*R*-BINOL[2], corresponding to enantioselectivity (K_S/K_R ratio) of 11.5 (Figures S28−S31 and Table 1). Similarly, for *S*-G1@*S*-BINOL[2] and *R*-G1@*S*-BINOL[2], the association constants were determined to be $(1.3 \pm 0.2) \times 10^3$ and $(1.4 \pm 0.3) \times 10^4$ M^{-1}, respectively, resulting in a comparable (if reciprocal) enantioselectivity (K_R/K_S ratio) of 10.8 (Figures S32−S35 and Table 1). These findings are consistent with the notion that *R*/*S*-BINOL[2] displays differential affinities for the enantiomers of *R*-G1 and *S*-G1 as initially inferred based on the qualitative studies discussed above.

Since the inward-directing OH (H_8) in host *R*/*S*-BINOL[2] was deemed important in stabilizing the observed host−guest binding interactions, the congeneric macrocyclic hosts with outward-facing OH moieties (*exo*-*R*/*S*-BINOL[2]) were also studied. When a $CDCl_3$ solution of *exo*-*R*/*S*-BINOL[2] was titrated with *R*/*S*-G1, no changes in the chemical shifts were observed for either the hosts or the guests (Figures S36−S38). This finding is taken as further support for the conclusion that the inward-directing OH groups present in *R*/*S*-BINOL[2] play a crucial role in mediating the observed guest recognition.

Further insights into the molecular recognition features leading to the enantioselectivity seen in the case of *S*/*R*-G1@*R*-BINOL[2] came from calculations. The energy-minimized structures of the two complexes were determined through energy minimization using density functional theory (DFT) at the B3LYP-D3/6-31G(d) level, taking into account solvent effects (Figure 4a,b)

Conformational searching revealed that each complex adopts the single most stable conformation independent of the initial arrangement of the host and guest. As shown in Figure 4a,b, the electronic binding energy of *S*-G1@*R*-BINOL[2] (ΔE = −164.56 kJ/mol) exceeds that of *R*-G1@*R*-BINOL[2] (ΔE = −152.99 kJ/mol), resulting in an energy difference of −11.57 kJ/mol. This observation aligns qualitatively with the results obtained from the ^{1}H NMR spectroscopic titrations, which yielded association constants of $(1.5 \pm 0.3) \times 10^4$ M^{-1} for *S*-G1@*R*-BINOL[2] and $(1.3 \pm 0.1) \times 10^3$ M^{-1} for *R*-G1@*R*-BINOL[2], as noted above.

The calculations also provide an energetic-based explanation for the enantioselective recognition seen by the experiment. In the calculated structures of the host−guest complexes, both *S*-G1 and *R*-G1 are positioned within the cavity of *R*-BINOL[2] and are effectively shielded; this finding is consistent with the significant upfield chemical shifts observed in the ^{1}H NMR spectra of *S*/*R*-G1 (vide spra). Moreover, multiple noncovalent interactions involving hydrogen bonding, $\pi\cdots\pi$ donor−acceptor, and C−H$\cdots\pi$ interactions were observed in the calculated structure of *S*-G1@*R*-BINOL[2]. For instance, the three methyl groups of the trimethylammonium moiety participate in four hydrogen bonding interactions with three OH groups of the host; the phenyl moiety of *S*-G1 engages in $\pi\cdots\pi$ donor−acceptor interactions with the naphthol unit of the host; the methyl in the stereogenic center points into the host cavity and participates in hydrogen bonding interactions with two OH moieties; the hydrogen atom in the chiral center is near one OH group of the host and interacts with it via an apparent hydrogen bonding interaction. In contrast, the conformation of *R*-G1@*R*-BINOL[2] is influenced by the reversed positions of the methyl groups and hydrogen atoms in the stereogenic center. This reversal leads to severe steric hindrance between the methyl and OH groups. As a consequence, *R*-G1 is displaced from the cavity and adopts a conformation with higher energy (11.57 kJ/mol) compared to *S*-G1@*R*-BINOL[2].

To gain further understanding of the molecular recognition behavior, the molecular electrostatic potentials (MEPs) on the molecular van der Waals surfaces of *R*-BINOL[2] and *S*-G1 were mapped (Figure 4c). The cavity of *R*-BINOL[2] is electron-rich, while *S*-G1 is electron-deficient, particularly in its trimethylammonium group. The optimized binding geometry was deemed reasonable since molecules tend to approach each other in a complementary manner, as reflected in the MEP. These findings highlight the significance of complementary fits and the presence of stabilizing noncovalent interactions between the host and bound guest molecules in governing the enantioselective recognition seen for *R*-BINOL[2] and guest *R*/*S*-G1.

Against the background presented above, we sought to explore the structural determinants that might underlie the relatively high enantioselectivity seen for *R*/*S*-G1. This was done through systematic structural changes in the guests. For instance, to explore the impact of aromatic groups on chiral selectivity, *R*/*S*-G2 and *R*/*S*-G3 were selected for the study. The K_R/K_S increased to 13.2 for *R*/*S*-G2 (from 11.5 for *R*/*S*-G1), thus revealing how the addition of aromatic groups may be used to increase the enantioselectivity (Figures S39−S50 and Table 1). On the other hand, a reduced K_R/K_S (2.5) is seen in the case of *R*/*S*-G3. This reduction is ascribed to steric hindrance and serves to highlight the importance of substituent positioning on the enantioselectivity (Figures S51−S62 and Table 1).

In the case of G2 for which high selectivity was observed, NMR spectroscopic experiments and DFT calculations were carried out. The ^{1}H NMR and ROESY results are similar to what was seen in the case of *R*/*S*-G1 above. For instance, more significant changes were observed in the proton signals of *S*-G2 compared to *R*-G2 ($\Delta\delta$ = −0.78 and −0.58 ppm for H_a, −1.09 and −0.63 ppm for H_b, and −0.63 and −0.40 ppm for H_c, respectively; Figure S39). In addition, NOE cross-peaks between H_a−H_2 in these complexes could be observed (Figures S63 and S64). DFT calculations on the *R*/*S*-G2@*R*-BINOL[2] complexes revealed the presence of multiple noncovalent interactions, including hydrogen bonding and C−H$\cdots\pi$ interactions (Figure S65). The *S*-G2@*R*-BINOL[2] exhibited a lower electronic binding energy (ΔE = −179.20 kJ/mol) compared to the *R*-G2@*R*-BINOL[2] (ΔE = −163.14 kJ/mol). These results are thus qualitatively aligned with the binding data obtained from ^{1}H NMR spectroscopic titrations.

We further tested guests in which the aromatic group in G1 was replaced with a pyridinium or an aliphatic ammonium

https://doi.org/10.1021/jacs.4c07924
J. Am. Chem. Soc. 2024, 146, 26233−26242

cation as well as ones in which the stereogenic center contains a hydroxyl substituent instead of a trimethylammonium group (guests *R*/*S*-G4, *R*/*S*-G5, and *R*/*S*-G6). However, the maximum enantioselectivity achieved was only 4.4 in the case of G4, with the remaining two values hovering around 2 (Figures S66−S89 and Table 1). This finding is interpreted in terms of the stereogenic trimethylammonium group playing a decisive role in producing high enantioselectivity in the case of the present receptor systems.

It is well appreciated that different drug enantiomers can differ dramatically in their pharmacological activity, metabolism, and toxicity.[6,76,77] For example, quinine and quinidine constitute a pair of enantiomers with completely different physiological activities. Quinine serves as an antimalarial drug, whereas quinidine acts as an antiarrhythmic drug.[78] We were thus keen to test whether the hosts of this study could be used to achieve the enantioselective recognition of representative drug enantiomers. With this objective in mind, we mixed the protonated products *R*-G7 and *S*-G7 with chiral hosts *R*/*S*-BINOL[2] in CD_2Cl_2 and monitored the changes produced by ^{1}H NMR spectroscopy. Distinct changes in the proton chemical shifts were seen for both the hosts and guests, providing qualitative evidence of enantioselective recognition (Figures S90 and S91). Job's plots and mass spectrometric studies supported a 1:1 binding stoichiometry (Figures S92 and S93). The association constants for these interactions ranged from $(5.0 \pm 0.4) \times 10^2$ to $(1.3 \pm 0.2) \times 10^3$ M^{-1}, resulting in K_R/K_S values of 1:2.4 for *R*-BINOL[2] and 2.5:1 for *S*-BINOL[2] (Figures S94−S101 and entries 13 and 14 in Table 1). While not appreciably high, these values demonstrate the potential of *R*/*S*-BINOL[2] and its analogs for the future chiral separation of drug enantiomers.

CONCLUSIONS

In summary, we successfully synthesized two pairs of chiral macrocycles, namely, *R*/*S*-BINOL[2] and *exo*-*R*/*S*-BINOL[2], through the Lewis acid-catalyzed reaction between the bis(2,4-dimethoxyphenyl)binaphthol monomer and paraformaldehyde. These macrocycles could be obtained in yields of up to 62% via a two-step process involving the use of commercially available starting materials. They could be purified by silica gel column chromatography without the need for chiral separation before use as receptors for chiral substrates. The macrocycles with inward-directing OH groups, namely, *R*/*S*-BINOL[2], exhibited highly enantioselective recognition toward chiral ammonium salts, with K_R/K_S values of up to 13.2 being obtained in the most favorable cases. In contrast, little recognition capacity was seen in the case of *exo*-*R*/*S*-BINOL[2], a finding ascribed to the absence of inward-directing OH groups. The enantioselective recognition achieved with *R*/*S*-BINOL[2] is attributed to a favorable steric matching between the host and guests, as well as stabilizing noncovalent interactions. The combination of a concise synthesis (two-step reaction sequence), good yields (up to 62%), high enantioselectivity (K_S/K_R up to 13.2), and a circumvented need to separate a racemic mixture of the receptors before use leads us to suggest that *R*/*S*-BINOL[2] may have a role to play in the recognition and separation of various chiral species.

ASSOCIATED CONTENT

Supporting Information

The Supporting Information is available free of charge at https://pubs.acs.org/doi/10.1021/jacs.4c07924.

Detailed synthetic procedures, crystallographic (corresponding to CCDC numbers 2338090 and 2338097), and spectroscopic (NMR, HRMS, fluorescence, and UV−vis spectra) characterization data for the macrocycles (PDF)

Accession Codes

CCDC 2338090 and 2338097 contain the supplementary crystallographic data for this paper. These data can be obtained free of charge via www.ccdc.cam.ac.uk/data_request/cif, or by emailing data_request@ccdc.cam.ac.uk, or by contacting The Cambridge Crystallographic Data Centre, 12 Union Road, Cambridge CB2 1EZ, UK; fax: +44 1223 336033.

AUTHOR INFORMATION

Corresponding Authors

Zhi-Yuan Zhang − *Academy of Interdisciplinary Studies on Intelligent Molecules, Tianjin Key Laboratory of Structure and Performance for Functional Molecules, College of Chemistry, Tianjin Normal University, Tianjin 300387, P.R. China*; orcid.org/0000-0001-9683-5034; Email: zzy@tjnu.edu.cn

Ming Dong − *Academy of Interdisciplinary Studies on Intelligent Molecules, Tianjin Key Laboratory of Structure and Performance for Functional Molecules, College of Chemistry, Tianjin Normal University, Tianjin 300387, P.R. China*; Email: hxxydongm@tjnu.edu.cn

Jonathan L. Sessler − *Department of Chemistry, The University of Texas at Austin, Austin, Texas 78712, United States*; orcid.org/0000-0002-9576-1325; Email: sessler@cm.utexas.edu

Chunju Li − *Academy of Interdisciplinary Studies on Intelligent Molecules, Tianjin Key Laboratory of Structure and Performance for Functional Molecules, College of Chemistry, Tianjin Normal University, Tianjin 300387, P.R. China*; orcid.org/0000-0001-7450-4867; Email: cjli@shu.edu.cn

Authors

Guang Sun − *Academy of Interdisciplinary Studies on Intelligent Molecules, Tianjin Key Laboratory of Structure and Performance for Functional Molecules, College of Chemistry, Tianjin Normal University, Tianjin 300387, P.R. China*; orcid.org/0009-0004-0120-9380

Xue Zhang − *Academy of Interdisciplinary Studies on Intelligent Molecules, Tianjin Key Laboratory of Structure and Performance for Functional Molecules, College of Chemistry, Tianjin Normal University, Tianjin 300387, P.R. China*; orcid.org/0009-0008-6205-1969

Zhe Zheng − *Academy of Interdisciplinary Studies on Intelligent Molecules, Tianjin Key Laboratory of Structure and Performance for Functional Molecules, College of Chemistry, Tianjin Normal University, Tianjin 300387, P.R. China*; orcid.org/0000-0003-0151-361X

Complete contact information is available at: https://pubs.acs.org/10.1021/jacs.4c07924

Notes

The authors declare no competing financial interest.

■ ACKNOWLEDGMENTS

The authors gratefully acknowledge the National Natural Science Foundation of China (21971192, 22201211, and 22301218), the Natural Science Foundation of Tianjin City (23JCZDJC00660 and 20JCZDJC00200). The work in Austin was supported by the National Science Foundation (CHE-2304731). Funding from the Robert A. Welch Foundation (F-0018 to J.L.S.) is also acknowledged.

■ REFERENCES

(1) Webb, T. H.; Wilcox, C. S. Enantioselective and diastereoselective molecular recognition of neutral molecules. *Chem. Soc. Rev.* **1993**, *22*, 383−395.
(2) Nguyen, H. V. T.; Jiang, Y.; Mohapatra, S.; Wang, W.; Barnes, J. C.; Oldenhuis, N. J.; Chen, K. K.; Axelrod, S.; Huang, Z.; Chen, Q.; Golder, M. R.; Young, K.; Suvlu, D.; Shen, Y.; Willard, A. P.; Hore, M. J. A.; Gómez-Bombarelli, R.; Johnson, J. A. Bottlebrush polymers with flexible enantiomeric side chains display differential biological properties. *Nat. Chem.* **2022**, *14*, 85−93.
(3) Cheng, Z.; Kuru, E.; Sachdeva, A.; Vendrell, M. Fluorescent amino acids as versatile building blocks for chemical biology. *Nat. Rev. Chem.* **2020**, *4*, 275−290.
(4) Liu, J.; Zhou, H.; Yang, W.; Ariga, K. Soft Nanoarchitectonics for Enantioselective Biosensing. *Acc. Chem. Res.* **2020**, *53*, 644−653.
(5) Vig, B. S.; Huttunen, K. M.; Laine, K.; Rautio, J. Amino acids as promoieties in prodrug design and development. *Adv. Drug. Deliver. Rev.* **2013**, *65*, 1370−1385.
(6) Brooks, W. H.; Guida, W. C.; Daniel, K. G. The Significance of Chirality in Drug Design and Development. *Curr. Top. Med. Chem.* **2011**, *11*, 760−770.
(7) Storch, G.; Trapp, O. By-design enantioselective self-amplification based on non-covalent product−catalyst interactions. *Nat. Chem.* **2017**, *9*, 179−187.
(8) Trost, B. M.; Chan, V. S.; Yamamoto, D. Enantioselective ProPhenol-Catalyzed Addition of 1,3-Diynes to Aldehydes to Generate Synthetically Versatile Building Blocks and Diyne Natural Products. *J. Am. Chem. Soc.* **2010**, *132*, 5186−5192.
(9) Jin, M. Y.; Zhen, Q.; Xiao, D.; Tao, G.; Xing, X.; Yu, P.; Xu, C. Engineered non-covalent π interactions as key elements for chiral recognition. *Nat. Commun.* **2022**, *13*, 3276.
(10) Metrano, A. J.; Chinn, A. J.; Shugrue, C. R.; Stone, E. A.; Kim, B.; Miller, S. J. Asymmetric Catalysis Mediated by Synthetic Peptides, Version 2.0: Expansion of Scope and Mechanisms. *Chem. Rev.* **2020**, *120*, 11479−11615.
(11) Schurig, V.; Betschinger, F. Metal-mediated enantioselective access to unfunctionalized aliphatic oxiranes: prochiral and chiral recognition. *Chem. Rev.* **1992**, *92*, 873−888.
(12) Phipps, R. J.; Hamilton, G. L.; Toste, F. D. The progression of chiral anions from concepts to applications in asymmetric catalysis. *Nat. Chem.* **2012**, *4*, 603−614.
(13) Wang, H.-F.; Zhu, Y.-Z.; Yan, X.-P.; Gao, R.-Y.; Zheng, J.-Y. A Room Temperature Ionic Liquid (RTIL)-Mediated, Non-Hydrolytic Sol−Gel Methodology to Prepare Molecularly Imprinted, Silica-Based Hybrid Monoliths for Chiral Separation. *Adv. Mater.* **2006**, *18*, 3266−3270.
(14) Navarro-Sánchez, J.; Argente-García, A. I.; Moliner-Martínez, Y.; Roca-Sanjuán, D.; Antypov, D.; Campíns-Falcó, P.; Rosseinsky, M. J.; Martí-Gastaldo, C. Peptide Metal−Organic Frameworks for Enantioselective Separation of Chiral Drugs. *J. Am. Chem. Soc.* **2017**, *139*, 4294−4297.
(15) Zhang, D.; Ronson, T. K.; Zou, Y.-Q.; Nitschke, J. R. Metal−organic cages for molecular separations. *Nat. Rev. Chem.* **2021**, *5*, 168−182.
(16) Das, S.; Xu, S.; Ben, T.; Qiu, S. Chiral Recognition and Separation by Chirality-Enriched Metal−Organic Frameworks. *Angew. Chem., Int. Ed.* **2018**, *57*, 8629−8633.
(17) Wang, Y.; Chen, J.-K.; Xiong, L.-X.; Wang, B.-J.; Xie, S.-M.; Zhang, J.-H.; Yuan, L.-M. Preparation of Novel Chiral Stationary Phases Based on the Chiral Porous Organic Cage by Thiol-ene Click Chemistry for Enantioseparation in HPLC. *Anal. Chem.* **2022**, *94*, 4961−4969.
(18) Pu, L. Simultaneous Determination of Concentration and Enantiomeric Composition in Fluorescent Sensing. *Acc. Chem. Res.* **2017**, *50*, 1032−1040.
(19) Rajasekar, P.; Jose, C.; Sarkar, M.; Boomishankar, R. Effective Enantioselective Recognition by Chiral Amino-Phosphonium Salts**. *Angew. Chem., Int. Ed.* **2021**, *60*, 4023−4027.
(20) Sutar, R. L.; Engelage, E.; Stoll, R.; Huber, S. M. Bidentate Chiral Bis(imidazolium)-Based Halogen-Bond Donors: Synthesis and Applications in Enantioselective Recognition and Catalysis. *Angew. Chem., Int. Ed.* **2020**, *59*, 6806−6810.
(21) Hu, M.; Feng, H.-T.; Yuan, Y.-X.; Zheng, Y.-S.; Tang, B. Z. Chiral AIEgens−Chiral recognition, CPL materials and other chiral applications. *Coord. Chem. Rev.* **2020**, *416*, No. 213329.
(22) Simonneaux, G.; Le Maux, P. Optically active ruthenium porphyrins: chiral recognition and asymmetric catalysis. *Coord. Chem. Rev.* **2002**, *228*, 43−60.
(23) Pu, L. Fluorescence of Organic Molecules in Chiral Recognition. *Chem. Rev.* **2004**, *104*, 1687−1716.
(24) Hu, M.; Ye, F.-Y.; Du, C.; Wang, W.; Yu, W.; Liu, M.; Zheng, Y.-S. Hindered Tetraphenylethylene Helicates: Chiral Fluorophores with Deep-Blue Emission, Multiple-Color CPL, and Chiral Recognition Ability. *Angew. Chem., Int. Ed.* **2022**, *61*, No. e202115216.
(25) Zhang, Q.; Toyoda, R.; Pfeifer, L.; Feringa, B. L. Architecture-Controllable Single-Crystal Helical Self-assembly of Small-Molecule Disulfides with Dynamic Chirality. *J. Am. Chem. Soc.* **2023**, *145*, 6976−6985.
(26) Noguchi, T.; Roy, B.; Yoshihara, D.; Sakamoto, J.; Yamamoto, T.; Shinkai, S. A Chiral Recognition System Orchestrated by Self-Assembly: Molecular Chirality, Self-Assembly Morphology, and Fluorescence Response. *Angew. Chem., Int. Ed.* **2017**, *56*, 12518−12522.
(27) Sethy, R.; Kumar, J.; Métivier, R.; Louis, M.; Nakatani, K.; Mecheri, N. M. T.; Subhakumari, A.; Thomas, K. G.; Kawai, T.; Nakashima, T. Enantioselective Light Harvesting with Perylenediimide Guests on Self-Assembled Chiral Naphthalenediimide Nanofibers. *Angew. Chem., Int. Ed.* **2017**, *56*, 15053−15057.
(28) Jia, J.-G.; Zhao, C.-C.; Wei, Y.-F.; Zhai, Z.-M.; Bao, S.-S.; Jacobson, A. J.; Ma, J.; Zheng, L.-M. Macroscopic Helical Assembly of One-Dimensional Coordination Polymers: Helicity Inversion Triggered by Solvent Isomerism. *J. Am. Chem. Soc.* **2023**, *145*, 23948−23962.
(29) Liu, G.; Humphrey, M. G.; Zhang, C.; Zhao, Y. Self-assembled stereomutation with supramolecular chirality inversion. *Chem. Soc. Rev.* **2023**, *52*, 4443−4487.
(30) Hasell, T.; Cooper, A. I. Porous organic cages: soluble, modular and molecular pores. *Nat. Rev. Mater.* **2016**, *1*, 16053.
(31) Zhang, S.-Y.; Fairen-Jimenez, D.; Zaworotko, M. J. Structural Elucidation of the Mechanism of Molecular Recognition in Chiral Crystalline Sponges. *Angew. Chem., Int. Ed.* **2020**, *59*, 17600−17606.
(32) Han, X.; Yuan, C.; Hou, B.; Liu, L.; Li, H.; Liu, Y.; Cui, Y. Chiral covalent organic frameworks: design, synthesis and property. *Chem. Soc. Rev.* **2020**, *49*, 6248−6272.
(33) Gong, W.; Chen, Z.; Dong, J.; Liu, Y.; Cui, Y. Chiral Metal−Organic Frameworks. *Chem. Rev.* **2022**, *122*, 9078−9144.
(34) Salikolimi, K.; Praveen, V. K.; Sudhakar, A. A.; Yamada, K.; Horimoto, N. N.; Ishida, Y. Helical supramolecular polymers with rationally designed binding sites for chiral guest recognition. *Nat. Commun.* **2020**, *11*, 2311.
(35) Wang, C.; Xu, L.; Zhou, L.; Liu, N.; Wu, Z.-Q. Asymmetric Living Supramolecular Polymerization: Precise Fabrication of One-Handed Helical Supramolecular Polymers. *Angew. Chem., Int. Ed.* **2022**, *61*, No. e202207028.
(36) García, F.; Gómez, R.; Sánchez, L. Chiral supramolecular polymers. *Chem. Soc. Rev.* **2023**, *52*, 7524−7548.
(37) Arabi, M.; Ostovan, A.; Wang, Y.; Mei, R.; Fu, L.; Li, J.; Wang, X.; Chen, L. Chiral molecular imprinting-based SERS detection

https://doi.org/10.1021/jacs.4c07924
J. Am. Chem. Soc. 2024, 146, 26233−26242

strategy for absolute enantiomeric discrimination. *Nat. Commun.* **2022**, *13*, 5757.
(38) Cram, D. J. The design of molecular hosts, guests, and their complexes. *J. Incl. Phenom.* **1988**, *6*, 397−413.
(39) Sawada, M.; Takai, Y.; Yamada, H.; Hirayama, S.; Kaneda, T.; Tanaka, T.; Kamada, K.; Mizooku, T.; Takeuchi, S. Chiral Recognition in Host-Guest Complexation Determined by the Enantiomer-Labeled Guest Method Using Fast Atom Bombardment Mass Spectrometry. *J. Am. Chem. Soc.* **1995**, *117*, 7726−7736.
(40) Dominique, P.; Schnurr, M.; Lewandowski, B. Chiral recognition of amino-acid esters by a glucose-derived macrocyclic receptor. *Chem. Commun.* **2021**, *57*, 3476−3479.
(41) Liu, Y.; Zhang, Q.; Crespi, S.; Chen, S.; Zhang, X.-K.; Xu, T.-Y.; Ma, C.-S.; Zhou, S.-W.; Shi, Z.-T.; Tian, H.; Feringa, B. L.; Qu, D.-H. Motorized Macrocycle: A Photo-responsive Host with Switchable and Stereoselective Guest Recognition. *Angew. Chem., Int. Ed.* **2021**, *60*, 16129−16138.
(42) Rekharsky, M. V.; Inoue, Y. Complexation Thermodynamics of Cyclodextrins. *Chem. Rev.* **1998**, *98*, 1875−1918.
(43) Huang, Q.; Jiang, L.; Liang, W.; Gui, J.; Xu, D.; Wu, W.; Nakai, Y.; Nishijima, M.; Fukuhara, G.; Mori, T.; Inoue, Y.; Yang, C. Inherently Chiral Azonia[6]helicene-Modified β-Cyclodextrin: Synthesis, Characterization, and Chirality Sensing of Underivatized Amino Acids in Water. *J. Org. Chem.* **2016**, *81*, 3430−3434.
(44) Chen, L.; Chen, Y.; Zhang, Y.; Liu, Y. Photo-Controllable Catalysis and Chiral Monosaccharide Recognition Induced by Cyclodextrin Derivatives. *Angew. Chem., Int. Ed.* **2021**, *60*, 7654−7658.
(45) Quan, J.; Nie, G.; Xue, H.; Luo, L.; Zhang, R.; Li, H. Macroscopic Chiral Recognition by Calix[4]arene-Based Host−Guest Interactions. *Chem.—Eur. J.* **2018**, *24*, 15502−15506.
(46) Qing, G.-Y.; He, Y.-B; Wang, F.; Qin, H.-J.; Hu, C.-G; Yang, X. Enantioselective Fluorescent Sensors for Chiral Carboxylates Based on Calix[4]arenes Bearing an L-Tryptophan Unit. *Eur. J. Org. Chem.* **2007**, *2007*, 1768−1778.
(47) Álvarez-Yebra, R.; López-Coll, R.; Galán-Masferrer, P.; Lledó, A. Enantioselective Molecular Recognition in a Flexible Self-Folding Cavitand. *Org. Lett.* **2023**, *25*, 3190−3194.
(48) Mutihac, L.; Lee, J. H.; Kim, J. S.; Vicens, J. Recognition of amino acids by functionalized calixarenes. *Chem. Soc. Rev.* **2011**, *40*, 2777−2796.
(49) Huang, W.-H.; Zavalij, P. Y.; Isaacs, L. Chiral Recognition inside a Chiral Cucurbituril. *Angew. Chem., Int. Ed.* **2007**, *46*, 7425−7427.
(50) Mandadapu, V.; Day, A. I.; Ghanem, A. Cucurbituril: Chiral Applications. *Chirality* **2014**, *26*, 712−723.
(51) Rekharsky, M. V.; Yamamura, H.; Inoue, C.; Kawai, M.; Osaka, I.; Arakawa, R.; Shiba, K.; Sato, A.; Ko, Y. H.; Selvapalam, N.; Kim, K.; Inoue, Y. Chiral Recognition in Cucurbituril Cavities. *J. Am. Chem. Soc.* **2006**, *128*, 14871−14880.
(52) Sokolov, J.; Šindelář, V. Chiral Bambusurils for Enantioselective Recognition of Carboxylate Anion Guests. *Chem.—Eur. J.* **2018**, *24*, 15482−15485.
(53) Zhang, G.-W.; Li, P.-F.; Meng, Z.; Wang, H.-X.; Han, Y.; Chen, C.-F. Triptycene-Based Chiral Macrocyclic Hosts for Highly Enantioselective Recognition of Chiral Guests Containing a Trimethylamino Group. *Angew. Chem., Int. Ed.* **2016**, *55*, 5304−5308.
(54) Nemat, S. J.; Jędrzejewska, H.; Prescimone, A.; Szumna, A.; Tiefenbacher, K. Catechol[4]arene: The Missing Chiral Member of the Calix[4]arene Family. *Org. Lett.* **2020**, *22*, 5506−5510.
(55) Liu, G.; Guo, S.; Liu, L.; Fan, Y.; Lian, Z.; Chen, X.; Jiang, H. Shape-Persistent Triptycene-Derived Pillar[6]arenes: Synthesis, Host−Guest Complexation, and Enantioselective Recognitions of Chiral Ammonium Salts. *J. Org. Chem.* **2023**, *88*, 10171−10179.
(56) Liu, C.; Jin, Y.; Qi, D.; Ding, X.; Ren, H.; Wang, H.; Jiang, J. Enantioselective assembly and recognition of heterochiral porous organic cages deduced from binary chiral components. *Chem. Sci.* **2022**, *13*, 7014−7020.
(57) Cui, D.-X.; Geng, Y.; Kou, J.-N.; Shan, G.-G.; Sun, C.-Y.; Zhang, K.-H.; Wang, X.-L.; Su, Z.-M. Chiral self-sorting and guest recognition of porous aromatic cages. *Nat. Commun.* **2022**, *13*, 4011.
(58) Ma, Y.-L.; Quan, M.; Lin, X.-L.; Cheng, Q.; Yao, H.; Yang, X.-R.; Li, M.-S.; Liu, W.-E.; Bai, L.-M.; Wang, R.; Jiang, W. Biomimetic Recognition of Organic Drug Molecules in Water by Amide Naphthotubes. *CCS Chem.* **2021**, *3*, 1078−1092.
(59) Weh, M.; Shoyama, K.; Würthner, F. Preferential molecular recognition of heterochiral guests within a cyclophane receptor. *Nat. Commun.* **2023**, *14*, 243.
(60) Gropp, C.; Quigley, B. L.; Diederich, F. Molecular Recognition with Resorcin[4]arene Cavitands: Switching, Halogen-Bonded Capsules, and Enantioselective Complexation. *J. Am. Chem. Soc.* **2018**, *140*, 2705−2717.
(61) Zeng, Z.; Qiu, W.; Xing, H.; Huang, Z. Sol-Gel-Derived Crown Ether Stationary Phase for Capillary Gas. *Anal. Sci.* **2000**, *16*, 851−854.
(62) Zeng, Z.; Qiu, W.; Huang, Z. Solid-Phase Microextraction Using Fused-Silica Fibers Coated with Sol−Gel-Derived Hydroxy-Crown Ether. *Anal. Chem.* **2001**, *73*, 2429−2436.
(63) Hartlieb, K. J.; Holcroft, J. M.; Moghadam, P. Z.; Vermeulen, N. A.; Algaradah, M. M.; Nassar, M. S.; Botros, Y. Y.; Snurr, R. Q.; Stoddart, J. F. CD-MOF: A Versatile Separation Medium. *J. Am. Chem. Soc.* **2016**, *138*, 2292−2301.
(64) Clark, C.; Somsen, G. W.; Kohler, I. *Chiral Separation by Capillary Electrophoresis and Capillary Electrophoresis−Mass Spectrometry. In Chiral Separations and Stereochemical Elucidation*; Cass, Q.; Tiritan, M. E.; Junior, J. M. B.; Barreiro, J. C., Eds.; John Wiley & Sons, Inc., 2023; pp 103−142.
(65) Ríos, P.; Mooibroek, T. J.; Carter, T. S.; Williams, C.; Wilson, M. R.; Crump, M. P.; Davis, A. P. Enantioselective carbohydrate recognition by synthetic lectins in water. *Chem. Sci.* **2017**, *8*, 4056−4061.
(66) Cheng, C.; Cai, Z.; Peng, X.-S.; Wong, H. N. C. Enantiomeric Recognition of Amino Acid Salts by Macrocyclic Crown Ethers Derived from Enantiomerically Pure 1,8,9,16-Tetrahydroxytetraphenylenes. *J. Org. Chem.* **2013**, *78*, 8562−8573.
(67) Han, C.; Li, H. Chiral Recognition of Amino Acids Based on Cyclodextrin-Capped Quantum Dots. *Small* **2008**, *4*, 1344−1350.
(68) Gropp, C.; Trapp, N.; Diederich, F. Alleno-Acetylenic Cage (AAC) Receptors: Chiroptical Switching and Enantioselective Complexation of trans-1,2-Dimethylcyclohexane in a Diaxial Conformation. *Angew. Chem., Int. Ed.* **2016**, *55*, 14444−14449.
(69) Han, X.-N.; Li, P. F.; Han, Y.; Chen, C.-F Enantiomeric Water-Soluble Octopus[3]arenes for Highly Enantioselective Recognition of Chiral Ammonium Salts in Water. *Angew. Chem., Int. Ed.* **2022**, *61*, No. e202202527.
(70) Yang, X.; Jiang, W. Enantioselective Recognition of Functional Organic Molecules in Water by Biomimetic Macrocyclic Hosts. *J. Am. Chem. Soc.* **2024**, *146*, 3900−3909.
(71) Fu, R.; Zhao, Q.-Y.; Han, H.; Li, W.-L.; Chen, F.-Y.; Tang, C.; Zhang, W.; Guo, S.-D.; Li, D.-Y.; Geng, W.-C.; Guo, D.-S.; Cai, K. A Chiral Emissive Conjugated Corral for High-Affinity and Highly Enantioselective Recognition in Water. *Angew. Chem., Int. Ed.* **2023**, *62*, No. e202315990.
(72) Zhang, Z.-Y.; Li, C. Biphen[n]arenes: Modular Synthesis, Customizable Cavity Sizes, and Diverse Skeletons. *Acc. Chem. Res.* **2022**, *55*, 916−929.
(73) Xu, K.; Li, B.; Yao, S.; Li, Z.; Lu, Y.; Dong, M.; Qiu, J.; Luo, L.; Li, C. Modular Introduction of endo-Binding Sites in a Macrocyclic Cavity towards Selective Recognition of Neutral Azacycles. *Angew. Chem., Int. Ed.* **2022**, *61*, No. e202203016.
(74) Zhao, Y.; Xiao, H.; Tung, C.-H.; Wu, L.-Z.; Cong, H. Adsorptive separation of cyclohexanol and cyclohexanone by nonporous adaptive crystals of RhombicArene. *Chem. Sci.* **2021**, *12*, 15528−15532.
(75) Li, S.; Liu, K.; Feng, X.-C.; Li, Z.-X.; Zhang, Z.-Y.; Wang, B.; Li, M.; Bai, Y.-L.; Cui, L.; Li, C. Synthesis and macrocyclization-induced

https://doi.org/10.1021/jacs.4c07924
J. Am. Chem. Soc. 2024, 146, 26233−26242

emission enhancement of benzothiadiazole-based macrocycle. *Nat. Commun.* **2022**, *13*, 2850.
(76) Nguyen, L. A.; He, H.; Pham-Huy, C. Chiral drugs: an overview. *Int. J. Biomed. Sci.* **2006**, *2*, 85−100.
(77) Kim, J. H.; Scialli, A. R. Thalidomide: The Tragedy of Birth Defects and the Effective Treatment of Disease. *Toxicol. Sci.* **2011**, *122*, 1−6.
(78) Achan, J.; Talisuna, A. O.; Erhart, A.; Yeka, A.; Tibenderana, J. K.; Baliraine, F. N.; Rosenthal, P. J.; D'Alessandro, U. Quinine, an old anti-malarial drug in a modern world: role in the treatment of malaria. *Malar. J.* **2011**, *10*, 144.

https://doi.org/10.1021/jacs.4c07924
J. Am. Chem. Soc. 2024, 146, 26233−26242